Scientia Iranica F (2019) 26(3), 1951–1961

Sharif University of Technology
Scientia Iranica
Transactions F: Nanotechnology
http://scientiairanica.sharif.edu

Structure, stability, and electronic properties of thin TiO_2 nanowires of different novel shapes: An *abs-initio* study

D. Dash[a*], C.K. Pandey[b], S. Chaudhury[b], and S.K. Tripathy[c]

a. *Department of ECE, Madanapalle Institute of Technology and Science, Madanapalle-517325, India.*
b. *Department of Electrical Engineering, NIT Silchar, Assam-788010, India.*
c. *Department of Electronics and Communication Engineering, NIT Silchar, Assam-788010, India.*

Received 16 May 2018; received in revised form 5 February 2019; accepted 4 March 2019

KEYWORDS
Nanostructures;
Ab initio calculations;
Electronic structure;
Density of states;
Bulk modulus.

Abstract. This paper investigates the structural stability and electronic properties of titanium dioxide (TiO_2) nanowires of different novel shapes using first-principle-based density functional approach. Among linear, ladder, saw tooth, square, triangular, hexagonal, and octahedron shaped atomic configurations, the ladder shape is the most energetically stable. After computation of lattice parameters as well as various mechanical properties of nanowire TiO_2, it was observed that the highest bulk modulus was related to triangular TiO_2 nanowire, which showed the highest mechanical strength of structure, whereas hexagonal configuration had the lowest bulk modulus, showing the lowest mechanical strength of structure. Analysis of various electronic properties showed that different configurations of TiO_2 nanowires could have different utilities as solid-state materials.

1. Introduction

In the past few decades, several families of nanostructures have been developed, including quantum dots, carbon nanotubes [1], zero-bandgap graphene, and semiconductor nanowires [2-5]. Each of the above materials exhibits many interesting properties. The main motivation for investigating a single material is to study its magnificent properties, although a specific single material with outstanding properties may not constitute a total new technology. Specifically, the potential to create new nanostructures and assembling with a tunable composition enables radical change in society and future technologies. In other words, in lieu of exploring a single nanomaterial, investigations can be carried out into systems in which different structures, shapes, compositions, and properties analogous to them can be tuned.

Considering the above facts, semiconductor nanowires [6,7] are among the most powerful quasi single dimensional (1D) platforms available in today's nano arena. Nanowire is an excellent 1D structure with electrical carriers in one direction and restricted in the other two directions. Nowadays, nanowires have numerous applications in different research areas like LASERs, sensitive polarized photodetectors, Light Emitting Diodes (LEDs), logic gates, various families of field effect transistors, renewable energy devices like solar cells, single-electron storage devices, single-hole transistors, lithium-ion storage batteries, and DNA detectors [8-13]. Yong Pan et al. investigated the intermediate product of Li_2S_2, which plays a key role in the charge/discharge process of Li-S batteries. They predicted two new Li_2S_2 phases, namely orthorhombic (Cmca) and orthorhombic (l mmm) structures, and

*. *Corresponding author. Tel.: +91 8249355210*
E-mail address: debashishdashnits@gmail.com (D. Dash)

doi: 10.24200/sci.2019.50644.1800

calculated average open circuit voltages (V_{oc}) and electronic properties of Li_2Si_2 [14]. As we know, nowadays, the world is faced with different problems due to consumption of fossil fuels, e.g., greenhouse effect, which causes global warming leading to sudden climatic changes. Thus, solar cells are the best alternative renewable energy sources. For producing solar cells, different materials are used, e.g., monocrystalline silicon [15], polycrystalline silicon [16], silicon thin film [17,18], cadmium telluride [19], copper indium gallium selenide [20], gallium nitride [21], gallium arsenide [22], etc. These materials can be used in producing solar cells with an efficiency of 14-19%, whereas the newly developed Dye Sensitized Solar Cells (DSSCs) have the efficiency of 32% under standard test conditions; moreover, a two-level tandem DSSC embodiment could reach 46% efficiency, according to Prof. Michael Graetzel, Ecole Polytechnique Federale de Lausanne (EPFL) [23]. These advanced solar cells are made of titanium dioxide, which is known for its non-toxicity, low cost, easy availability, long-term stability, and superb photo catalytic nature [24,25]. Pan [26] investigated a hydrogen storage mechanism and developed the hydrogen storage capacity using hydrogen diffusion mechanism and hydrogenation processing through MoS_2 with S-S interlayer. Then, Pan and Guan [27] investigated MoS_3 as a potential hydrogen storage material due to the interaction between hydrogen and unsaturated sulphur atoms. They studied the structure as well as relevant physical and thermodynamic properties of MoS_3 and calculated phonon dispersion, electronic structure, band structure, and heat capacity. Further, they investigated Molybdenum sulphides. They found out that MoS with hexagonal structure was more thermodynamically stable due to the charge distribution with increasing S concentration. They also concluded that the elastic properties were dependent on S concentration [28]. TiO_2 has natural and high pressure phases; natural TiO_2 is a wide-bandgap semiconductor, whereas high-pressure TiO_2 is perfect for making renewable panels. TiO_2 was comprehensively investigated as a photo anode for photo electrochemical (PEC) water splitting by Fujishima and Honda [29]. They found out TiO_2 had great photo catalytic activity, proper band edge positions, and superior photo chemical stability. Many research groups have conducted experiments on TiO_2 nanowires by implementing various experimental procedures. Bin Wu et al. [30] reported solvothermal synthesis of natural anatase TiO_2 nanowires in a large quantity, which showed outstanding photo catalytic activity in the degradation of Rhodamine B. TiO_2 has also been used to improve the efficiency of various solar cells; in addition, it can be utilized to improve the performance of gas sensors. Despite all the mentioned studies, which provide some interesting results about TiO_2, few research groups have studied the transfer properties of 1D TiO_2 nanostructures.

Many groups have performed a large number of experiments on TiO_2 synthesis and growth aspect, but stability and various electronic properties of different sizes and shapes have not been checked, either experimentally or theoretically, by any researcher. It is a fact known to all that in nanometer regimes, geometrical shape and structure play an important role in various changes of the electronic and other properties [31]. Many researchers have performed theoretical calculations on different shapes and structures of other materials like gallium phosphide (GaP) [32], gallium nitride (GaN) [11], gallium arsenide (GaAs) [11], gallium antimonite (GaSb) [11], aluminum phosphide (AlP) [33], aluminum arsenide (AlAs) [33], and aluminum antimonite (AlSb) [33] nanowires. However, none of them worked on proper theoretical investigation into different shapes of the titanium dioxide (TiO_2) nanowires. Tafen et al. [34] investigated four types of small-perimeter TiO_2 nanowires with round, octagonal, hexagonal, and square shapes along the 'z' direction. They found that, except for the square structure, all other structures were stable in nature. However, besides these four shapes, there are many more shapes of TiO_2 nanowires, which have not been investigated yet. This motivated us to consider different shapes and investigate stability and various electronic properties of every single shape of thin nanowires containing up to 6 atoms. The band structure and density of states are thoroughly analyzed for all shapes of nanowires.

2. Computational details

All the simulations have been carried out within the framework of Density Functional Theory (DFT) [35,36], which is the basic theory used to find out properties of any material. In this paper, seven different shapes of TiO_2, namely linear, zigzag, ladder, square, triangular, hexagonal, and octahedron, are considered. The popular Atomistix Tool Kit (ATK) [37] has been employed for optimization of different geometrical shapes performed in Limited memory Broyden-Fletcher-Goldfarb-Shanno (LBFGS) [38-41] approximation. The generalized gradient approximation [42,43] with Revised Perdew, Burke, and Ernzerhof (RevPBE) is used as an exchange correlation potential. ATK is an advanced version of the previously available TranSIESTA-C [44,45], which is based on the new molecular technology, models, and various algorithms developed in the platform of TranSIESTA. Some part of this tool has been developed using McDAL [46], which employs different localized basis sets developed earlier in SIESTA [47]. Here, using supercell technique, nanowires are placed in the 'z' direction. The linear,

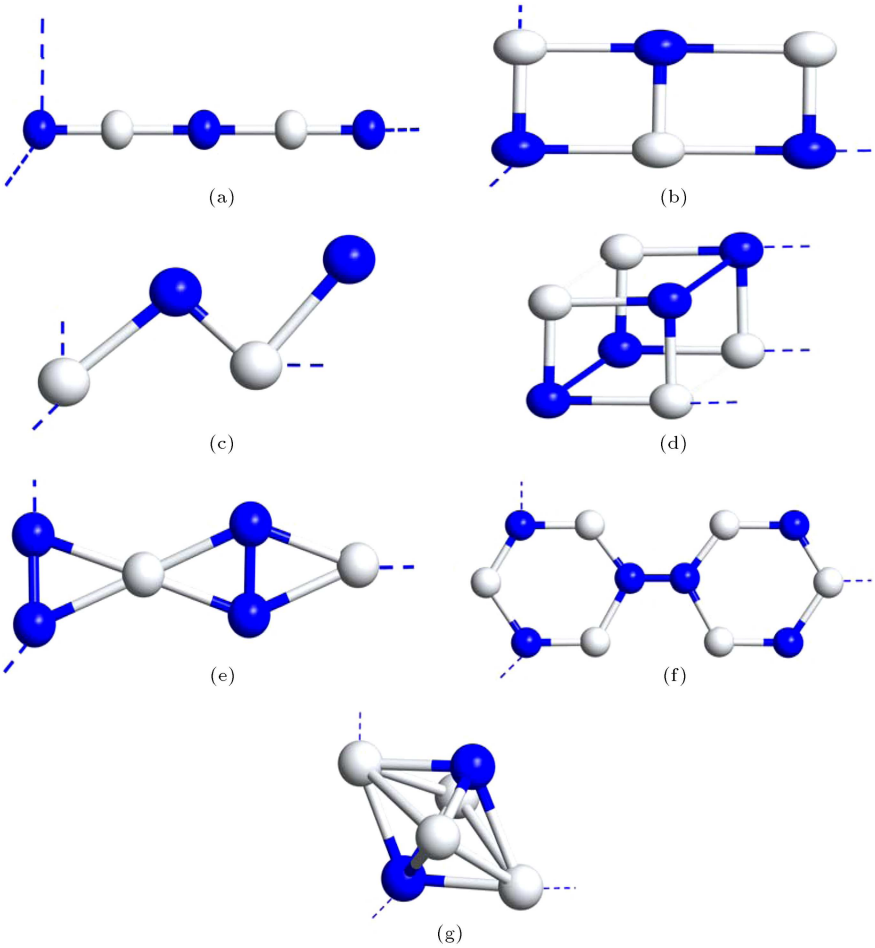

Figure 1. Atomic configurations of TiO_2 nanowires: (a) Linear, (b) ladder, (c) saw tooth, (d) square, (e) triangular, (f) hexagonal, and (g) octahedron (blue atoms are O and white atoms are Ti).

ladder, saw tooth, square, triangular, hexagonal, and octahedron configurations of TiO_2 nanowires, which are considered here for simulation, are shown in Figure 1. The cut-off energy is considered as 100 Ry and the first Brillouin-zone integration is considered with a Monkhorst-Pack scheme using $1\times1\times5$ k-points. The cut-off energy and the number of k-points are continuously changed to find out convergence under the force tolerance having the value of 0.05 eVÅ^{-1} for the various values reported here.

3. Results and discussion

3.1. Stability analysis

First, stability analysis is carried out on titanium dioxide nanowires for different configurations, such as linear, ladder, saw tooth, square, triangular, hexagonal, and octahedron, in which the equilibrium lattice constant is obtained by minimizing the total energy in a self-consistent manner. Figure 2 shows the plot of total energy expressed in 'eV' versus total volume expressed in 'Ang^3' for all the nanowires with different atomic configurations. In Figure 2, it can be observed that the ladder shaped nanowire configuration has the lowest energy; this implies that it can be the most stable configuration among all configurations. The bond lengths of all the 7 structures of nanowires have been computed and listed in Table 1. As we know, bulk and shear moduli are the parameters for the measurement of hardness of any crystalline solid. Many researchers worked on the elastic moduli of different types of coating materials. Pan and Wen [48] investigated structural stability and mechanical properties of IrAl coating. They showed that vacancy mechanism played an important role in improving Vickers hardness of IrAl coating. Further, Pan [26] studied four $RuAl_2$ structures and predicted their electronic and mechanical properties. It was observed that among the 4 $RuAl_2$ structures, namely $TiSi_2$, $TiAl_2$, $OsAl_2$, and $AuAl_2$, $TiSi_2$ behaved like a semiconductor and the other three had metal-like nature. He also studied their elastic properties using bond length and shear information [49,50]. Similarly, Pan et al. [51] investigated structural and mechanical properties of PtAlTM ternary alloy in a first-principle manner. Furthermore, Pan et al. [52] investigated crystal structure, elastic

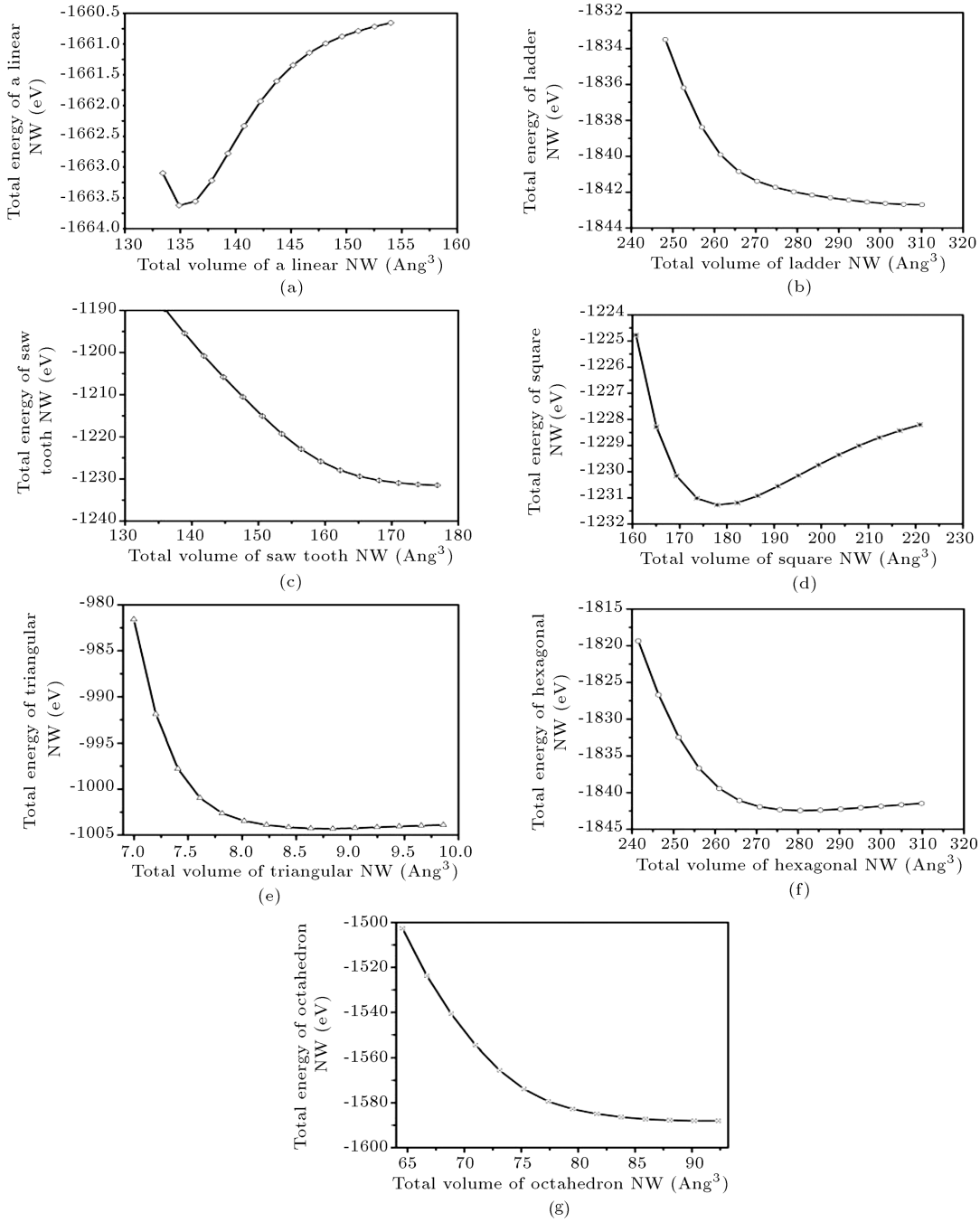

Figure 2. Total energy versus total volume of (a) linear NW, (b) ladder NW, (c) saw tooth NW, (d) square NW, (e) triangular NW, (f) hexagonal NW, and (g) octahedron NW.

Table 1. Atomic configuration, bond length expressed in Ang., and various mechanical properties of bulk modulus (B), shear modulus (G), and Young's modulus (Y).

Structure	Bond length (Å)	Mechanical properties		
		B	G	Y
Linear	2.09	27.42	6.95	316.3
Ladder	2.05	-12.69	69.79	3.20
Saw tooth	2.23	22.97	10.84	56.78
Square	2.15	13.20	9.94	76.79
Triangular	2.19	3792	2131	2285
Hexagonal	1.82	4.00	2.96	40.86
Octahedron	2.25	85.6674	61.6739	-230

properties, Vickers hardness, elastic anisotropy, and electronic and thermodynamic properties of transition metal silicides like Mo_5Si_3. Here, the results of simulations of bulk, shear, and Young's moduli for different structures of TiO_2 nanowires are shown in Table 1 and analysed briefly. In Table 1, it can be observed that hexagonal structure has the lowest and triangular structure has the highest stiffness.

3.2. Electronic properties

The band diagrams of TiO_2 nanowires for different shapes are shown in Figure 3 along with other mechanical properties, like bulk modulus, shear modulus, and Young's modulus. All the moduli for each configuration of nanowires are found out by the 1-D analogy of Murnaghan equation of state [53]. Mathematically, it can be given as in Eq. (1):

$$P(V) = \frac{3B_0}{2}\left[\left(\frac{V_0^{\frac{7}{3}}}{V}\right) - \left(\frac{V_0^{\frac{5}{3}}}{V}\right)\right] \left\{1 + \frac{3}{4}(B_0' - 4)\left[\left(\frac{V_0^{\frac{2}{3}}}{V}\right) - 1\right]\right\}, \quad (1)$$

where P is Pressure, V_0 reference volume, V deformed volume, B_o bulk modulus, and B_o' derivative of the bulk modulus with respect to pressure.

It can be observed that all nanowire configurations have indirect bandgap except saw tooth structure. Furthermore, in Figure 3(a), it can be observed that linear structure has a narrow bandgap of 0.48 eV between Γ and Z points. It can also be observed that no conduction band crosses the Fermi level, which confirms that linear structured nanowire is not metallic in nature. However, some of the conduction bands are very much close to Fermi level, which means that linear nanowire can be a good semiconductor. In Figure 3(b), the band diagram of ladder-type nanowire shows a nominal bandgap of 0.028 eV and the transition occurs indirectly from Γ to Z. The bandgap mainly depends on the number of atoms taken into consideration and the pseudopotential taken for computation. In ladder-structure nanowire, one conduction band crosses the Fermi level in the band diagram, as shown in Figure 3(b). Thus, the ladder-type nanowire is metallic in nature. Figure 3(c) shows the band diagram of saw-tooth nanowire having a small bandgap of 0.094 eV; interestingly, transition occurs directly at point Z. As none of the conduction bands crosses the Fermi level, this nanowire structure can be considered as semiconductor. Similarly, in Figure 3(d), the band diagram of square structured nanowire can be studied. It is observed that four valence bands cross the Fermi energy level, proving that square-type nanowire is purely metallic in nature. Also, in Figure 3(e), it can be seen that triangular nanowire has a large bandgap of 11.5 eV and is indirect in nature. Therefore, due to its large bandgap, triangular nanowire can be categorized as an insulator. On the other hand, hexagonal nanowire has a small indirect bandgap of 0.13 eV, as shown in Figure 3(f), and is classifies as a semiconductor. Lastly, the band diagram of octahedron-type TiO_2 nanowire can be observed in Figure 3(g). As fabricated TiO_2 nanowires [54] are of octahedron type, it is absolutely necessary to analyse electronic structure of this type. As observed in the figure, octahedron-type NW is purely semiconducting in nature and has a direct bandgap of 0.17 eV.

The Total Density Of States (TDOS) and Partial Density Of States (PDOS) are important properties to study and analyse the electronic properties of a material. The TDOS and PDOS for each of the nanowire configurations are shown in Figure 4 and Figure 5. It can be seen in Figure 4(a) that there is a small peak in valence band region and two prominent peaks occur in the conduction band region. The peak that occurs at 0.6 eV has the highest magnitude and is much closer to Fermi level. It confirms that considerable localization of states occurs near the Fermi level. Both peaks can be seen in PDOS plot of linear nanowire, as shown in Figure 5(a). Similarly, Figures 4(b) and 5(b) show the TDOS and PDOS in ladder structured nanowire. In the figure, it is seen that two peaks occur in the valence band region near -17.2 and -3.5 eV. But, the highest peak occurs at 0.9 eV, which lies in the conduction band region. As this peak is much closer to the Fermi level, localization of states is highly close to Fermi level. Both the peaks are proved by the PDOS plot of ladder nanowire. Similarly, the TDOS and PDOS of saw tooth can be seen in Figures 4(c) and 5(c). Here, 2 prominent peaks are observed in the valence band region at -19.6 and -5.6 eV. However, like in the ladder-shape nanowires, the highest peak occurs near 1.5 eV in the conduction band region, which shows that the allowed states are much closer to the Fermi level. The same can be observed in PDOS plot as shown in Figure 5(c). For the square-shape nanowire, TDOS and PDOS are shown in Figures 4(d) and 5(d), respectively. Figure 4(d) demonstrates that two peaks are near -19.1 and -5.2 eV in the valence band region and one peak with the highest magnitude occurs in conduction band region at 1.3 eV. As this peak is also very close to the Fermi region, it proves that the allowed states are very close to Fermi level. The same can be observed in PDOS, as shown in Figure 5(d). The TDOS and PDOS of the triangular-shape nanowire are also depicted in Figures 4(e) and 5(e). It can be seen in Figure 4(e) that there is only one peak in the valence band region at -40 eV and two peaks in conduction band region at 30 and 40 eV. This indicates that there is less localization of allowed states near Fermi level. Thus, the triangular structured TiO_2

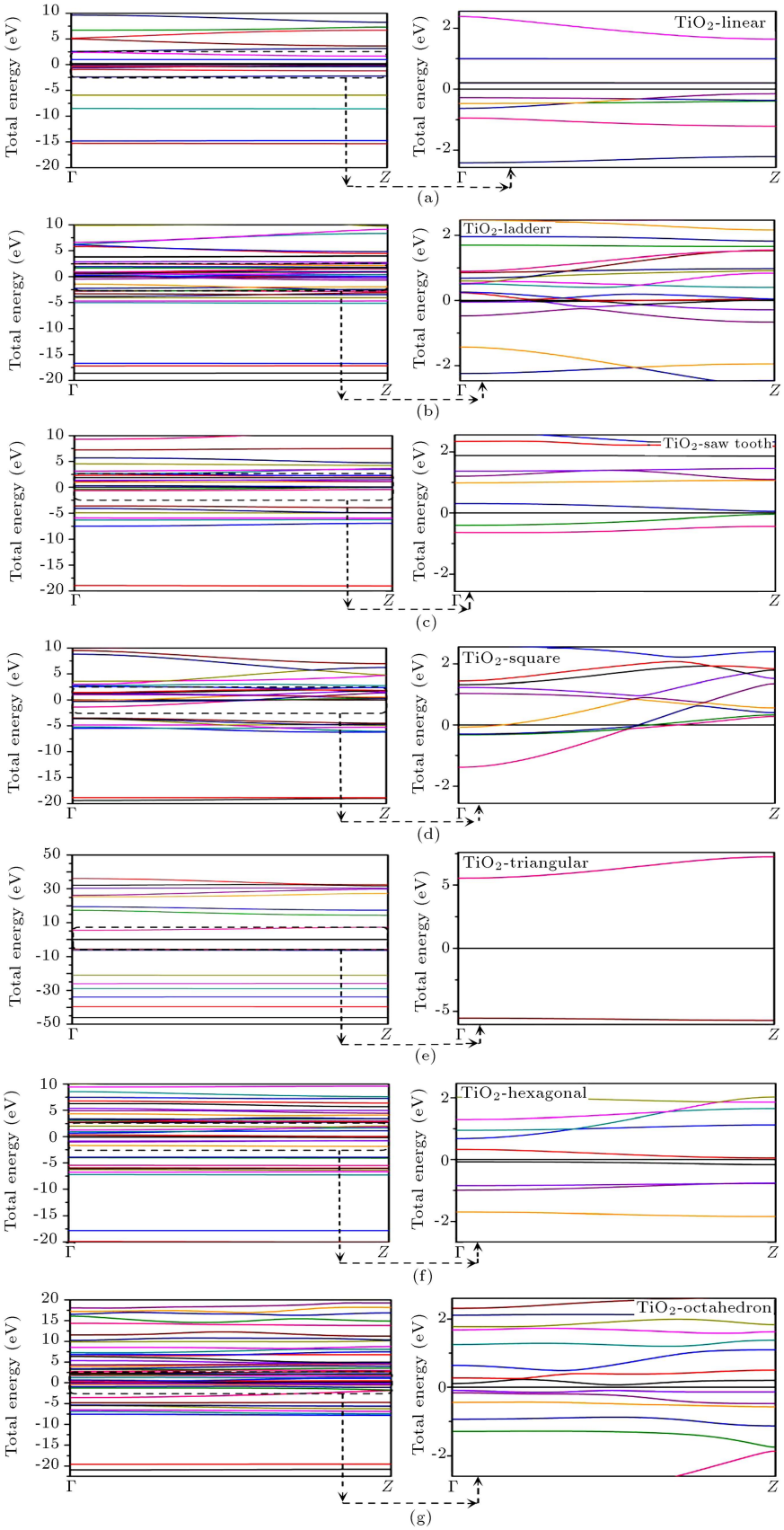

Figure 3. Band diagram of (a) linear NW, (b) ladder NW (c), saw tooth NW, (d) square NW, (e) triangular NW, (f) hexagonal NW, and (g) octahedron NW.

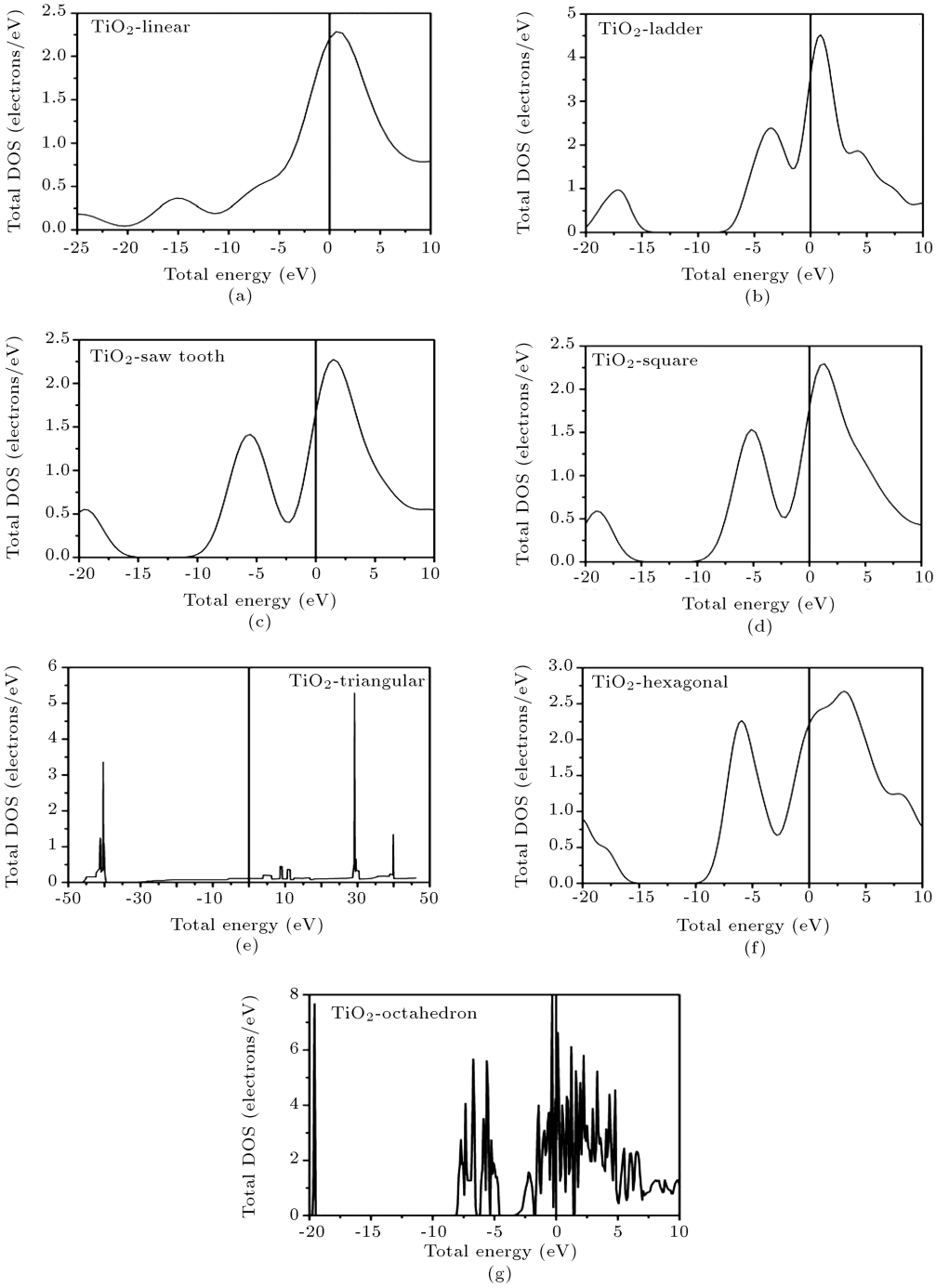

Figure 4. Density of states diagram for (a) linear TiO_2 NW, (b) ladder TiO_2 NW, (c) saw tooth TiO_2 NW, (d) square TiO_2 NW, (e) triangular TiO_2 NW, (f) hexagonal TiO_2 NW, and (g) octahedron TiO_2 NW.

nanowire can be used for the purpose of insulation, as also observed in its PDOS plot shown in Figure 5(e). The DOS for hexagonal shaped nanowire is shown in Figures 4(f) and 5(f). It can be seen that there are two prominent peaks, which occur in the valence band region. The peaks are placed at -20.2 and -5.9 eV. Two other peaks also occur in the conduction band region at 3.1 and 21.7 eV. Thus, the allowed states are close to the Fermi level; also, localization occurs, which can be observed in the PDOS plot provided in Figure 5(f). Finally, the total density and partial density of states for octahedron-type NW are shown in Figures 4(g) and 5(g). In both plots, it is seen that octahedron-type NW is of pure semiconductor type. A great number of peaks are seen in the conduction band, which prove the heavy localization of allowed states near the Fermi region. Thus, octahedron TiO_2 nanowire can best be used in different semiconductor applications.

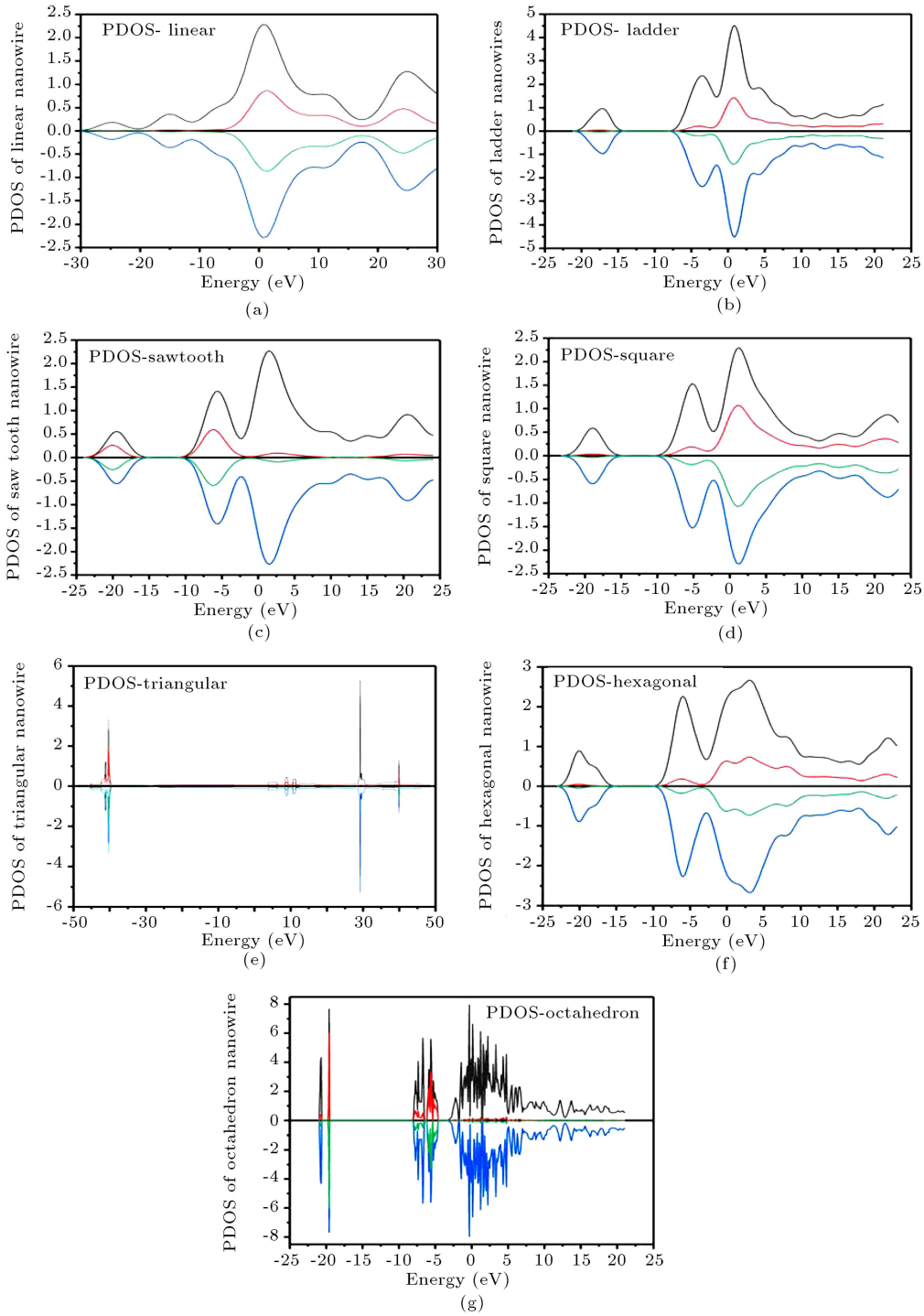

Figure 5. Partial density of states diagram for (a) linear TiO_2 NW, (b) ladder TiO_2 NW, (c) saw tooth TiO_2 NW, (d) square TiO_2 NW, (e) triangular TiO_2 NW, (f) hexagonal TiO_2 NW, and (g) octahedron TiO_2 NW.

4. Conclusion

In this paper, a DFT-based first-principle method was implemented to investigate the structural stability of TiO_2 nanowires with different atomic configurations. The ladder structure was found to be the most energetically stable configuration and triangular shaped TiO_2 nanowire had highest bulk modulus, confirming its highest elastic strength among all configurations. Ladder and hexagonal shaped atomic configurations had very low bulk modulus, which proved softening of the material if dimensions were reduced. Linear, saw tooth, and hexagonal shaped atomic configurations showed semiconducting nature, whereas ladder

and square shaped nanowires had metallic nature; the triangular shaped nanowire behaved as a pure insulator. Finally, octahedron nanowire had neither low nor high bulk modulus, which proved that it was a semiconducting material.

Acknowledgement

The authors are thankful to Professor Sivaji Bandyopadhyay, Director of the National Institute of Technology, Silchar, Assam, for his continuous support of this work.

References

1. Nouri, N. and Ziaei-Rad, S. "Mechanical property evaluation of carbon nanotube sheets", *Sci. Iran.*, **17**(2), pp. 90-101 (2010).
2. Sinha, S.K. and Chaudhury, S. "Impact of oxide thickness on gate capacitance - A comprehensive analysis on MOSFET, nanowire FET, and CNTFET devices", *IEEE Trans. Nanotechnol.*, **12**(6), pp. 958-964 (2013).
3. Sinha, S.K. and Chaudhury, S. "Comparative study of leakage power in CNTFET over MOSFET device", *J. Semicond.*, **35**, 114002 (2014).
4. Rezania, H., Goli, S., and Jazideh, A. "Electrical conductivity of doped armchair graphene nanoribbon in the presence of gap parameter", *Sci. Iran.*, **25**(3), pp. 1808-1814 (2018).
5. Mohammadzadeh Honarvar, F., Pourabbas, B., Salami Hosseini, M., Kharazi, M., and Erfan-Niya, H. "Molecular dynamics simulation: The effect of graphene on the mechanical properties of epoxy based photoresist: SU8", *Sci. Iran.*, **25**(3), pp. 1879-1890 (2018).
6. Lieber, C.M. "Semiconductor nanowires: A platform for nanoscience and nanotechnology", *MRS Bulletin*, **36**, pp. 1052-1063 (2011).
7. Lu, W. and Lieber, C.M. "Semiconductor nanowires", *J. Phys. D-Applied Phys.*, **39**(21), pp. R387-R406 (2006).
8. Zhang, W., Zhu, R., Liu, X., Liu, B., and Ramakrishna, S. "Facile construction of nanofibrous ZnO photoelectrode for dye-sensitized solar cell applications", *Appl. Phys. Lett.*, **95**(4), pp. 2-5 (2009).
9. Zuruzi, A.S., Kolmakov, A., MacDonald, N.C., and Moskovits, M. "Highly sensitive gas sensor based on integrated titania nanosponge arrays", *Appl. Phys. Lett.*, **88**(10), pp. 102904-102906 (2006).
10. O'Regan, B. and Grätzel, M. "A low-cost, high-efficiency solar cell based on dye-sensitized colloidal TiO_2 films", *Nature*, **353**(6346), pp. 737-740 (1991).
11. Srivastava, A., Tyagi, N., and Ahuja, R. "First-principles study of structural and electronic properties of gallium based nanowires", *Solid State Sci.*, **23**, pp. 35-41 (2013).
12. Wang, J., Gudiksen, M.S., Duan, X., Cui, Y., and Lieber, C.M. "Highly polarized photoluminescence and photodetection from single indium phosphide nanowires", *Science*, **293**(5534), pp. 1455-1457 (2001).
13. Yanson, A.I., Rubio Bollinger, G., Van Den Brom, H.E., Agraït, N., and Van Ruitenbeek, J.M. "Formation and manipulation of a metallic wire of single gold atoms", *Nature*, **395**(6704), pp. 783-785 (1998).
14. Pan, Y. and Guan, W.M. "Prediction of new phase and electrochemical properties of Li_2S_2 for the application of Li-S batteries", *Inorg. Chem.*, **57**(11), pp. 6617-6623 (2018).
15. Chander, S., Purohit, A., Sharma, A., Nehra, S.P., and Dhaka, M.S. "Impact of temperature on performance of series and parallel connected mono-crystalline silicon solar cells", *Energy Reports*, **1**, pp. 175-180 (2015).
16. Becker, C. "Polycrystalline silicon thin-film solar cells: Status and perspectives", *Sol. Energy Mater. Sol. Cells*, **119**, pp. 112-123 (2013).
17. Meillaud, F. "Recent advances and remaining challenges in thin-film silicon photovoltaic technology", *Mater. Today*, **18**(7), pp. 378-384 (2015).
18. Müller, J., Rech, B., Springer, J., and Vanecek, M. "TCO and light trapping in silicon thin film solar cells", *Sol. Energy*, **77**, pp. 917-930 (2004).
19. Poplawsky, J.D. "Cadmium telluride solar cells: Record-breaking voltages", *Nat. Energy*, **1**(3), p. 16021 (2016).
20. Ramanujam, J. and Singh, U.P. "Copper indium gallium selenide based solar cells-a review", *Energy Environ. Sci.*, **10**, pp. 1306-1319 (2017).
21. Routray, S., Shougaijam, B., and Lenka, T.R. "Exploiting polarization charges for high-performance (000-1) facet GaN/InGaN/GaN Core/Shell/Shell tringular nanowire solar cell", *IEEE J. Quantum Electron.*, **53**(5), pp. 1-8 (2017).
22. Blakemore, J.S. "Semiconducting and other major properties of gallium arsenide", *J. Appl. Phys.*, **53**, p. R123 (1982).
23. Grätzel, M. "Dye-sensitized solar cells", *Journal of Photochemistry and Photobiology C: Photochemistry Reviews*, **4**(2). pp. 145-153 (2003).
24. Dash, D., Pandey, C.K., Chaudhury, S., and Tripathy, S.K. "Structural, electronic, and mechanical properties of cubic TiO_2: A first-principles study", *Chinese Phys. B*, **27**(1), pp. 1-9 (2018).
25. Dash, D., Chaudhury, S., and Tripathy, S.K. "First principle investigation of structural and optical properties of cubic titanium dioxide", in *AIP Conference Proceedings*, **1953**(1) (2018).
26. Pan, Y. "Role of S-S interlayer spacing on the hydrogen storage mechanism of MoS_2", *Int. J. Hydrogen Energy*, **43**(6), pp. 3087-3091 (2018).

27. Pan, Y. and Guan, W. "Prediction of new stable structure, promising electronic and thermodynamic properties of MoS_3 : Ab initio calculations", *J. Power Sources*, **325**, pp. 246-251 (2016).
28. Pan, Y. and Guan, W. "Effect of sulfur concentration on structural, elastic and electronic properties of molybdenum sulfides from first-principles", *Int. J. Hydrogen Energy*, **41**, pp. 11033-11041 (2016).
29. Fujishima, A. and Honda, K. "Electrochemical photolysis of water at a semiconductor electrode", *Nature*, **238**(5358), pp. 37-38 (1972).
30. Bin Wu, H., Chen, J.S., Hng, H.H., Wen, D., and Lou, X. "Nanostructured metal oxide-based materials as advanced anodes for lithium-ion batteries", *Nanoscale*, **4**, pp. 2526-2542 (2012).
31. Zhang, Q., Sun, C., Yan, J., Hu, X., Zhou, S., and Chen, P. "Perpendicular rutile nanosheets on anatase nano fibers: Heterostructured TiO_2 nanocomposites via a mild solvothermal method", *Solid State Sci.*, **12**(7), pp. 1274-1277 (2010).
32. Srivastava, P. and Singh, S. "Electronic properties of GaP nanowires of different shapes", *J. Nanosci. Nanotechnol.*, **11**(12), pp. 10464-10469 (2011).
33. Srivastava, A. and Tyagi, N. "Structural and electronic properties of AlX (X=P, As, Sb) nanowires: Ab initio study", *Mater. Chem. Phys.*, **137**(1), pp. 103-112 (2012).
34. Tafen, D. and Lewis, J. "Structure, stability, and electronic properties of thin TiO_2 nanowires", *Phys. Rev. B*, **80**(1), pp. 014104-014108 (2009).
35. Hohenberg, P. and Kohn, W. "The inhomogeneous electron gas", *Phys. Rev.*, **136**(3B), p. B864 (1964).
36. Kohn, W. and Sham, L.J. "Self-consistent equations including exchange and correlation effects", *Phys. Rev.*, **140**, p. A1133 (1965).
37. Dash, D., Chaudhury, S., and Tripathy, S.K. "A density functional theory-based study of electronic and optical properties of anatase titanium dioxide", *Advances in Communication, Devices, and Networking*, Lecture Notes on Electrical Engineering, **462**, pp. 57-67 (2018).
38. Broyden, C.G. "The convergence of a class of double-rank minimization algorithms 1. General considerations", *IMA J. Appl. Math. (Institute Math. Its Appl.*, **6**(1), pp. 76-90 (1970).
39. Fletcher, R. "A new approach to variable metric algorithms", *Comput. J.*, **13**(3), pp. 317-322 (1970).
40. Goldfarb, D. "A family of variable-metric methods derived by variational means", *Math. Comput.*, **24**, pp. 23-26 (1970).
41. Shanno, D.F. and Kettler, P.C. "Optimal conditioning of quasi-Newton methods", *Math. Comput.*, **24**, pp. 657-664 (1970).
42. Zhang, Y. and Yang, W. "Comment on 'generalized gradient approximation made simple", *Physical Review Letters*, **80**, p. 890 (1998).
43. Hammer, B., Hansen, L.B., and Nørskov, J.K. "Improved adsorption energetics within density-functional theory using revised Perdew-Burke-Ernzerhof functionals", *Phys. Rev. B-Condens. Matter Mater. Phys.*, **59**, p. 7413 (1999).
44. Brandbyge, M., Mozos, J.L., Ordejón, P., Taylor, J., and Stokbro, K. "Density-functional method for nonequilibrium electron transport", *Phys. Rev. B-Condens. Matter Mater. Phys.*, **65**(16), p. 165401 (2002).
45. Stokbro, K., Taylor, J., Brandbyge, M., and Ordejón, P. "TranSIESTA: A spice for molecular electronics", in *Annals of the New York Academy of Sciences*, **1006**, pp. 212-226 (2003).
46. Taylor, J., Guo, H., and Wang, J. "Ab initio modeling of quantum transport properties of molecular electronic devices", *Phys. Rev. B*, **63**, p. 245407 (2001).
47. Soler, J.M. "The SIESTA method for abs initio order-N materials simulation", *J. Phys. Condens. Matter*, **14**(11), pp. 2745-2779 (2002).
48. Pan, Y. and Wen, M. "The influence of vacancy on the mechanical properties of IrAl coating: First-principles calculations", *Thin Solid Films*, **664**, pp. 46-51 (2018).
49. Pan, Y. "$RuAl_2$: Structure, electronic and elastic properties from first-principles", *Mater. Res. Bull.*, **93**, pp. 56-62 (2017).
50. Pan, Y. and Jin, C. "Vacancy-induced mechanical and thermodynamic properties of B2-RuAl", *Vacuum*, **143**, pp. 165-168 (2017).
51. Pan, Y., Wang, S.L., and Zhang, C.M. "Ab-initio investigation of structure and mechanical properties of PtAlTM ternary alloy", *Vacuum*, **151**, pp. 205-208 (2018).
52. Pan, Y., Wang, P., and Zhang, C.M. "Structure, mechanical, electronic and thermodynamic properties of Mo_5Si_3 from first-principles calculations", *Ceram. Int.*, **44**(11), pp. 12357-12362 (2018).
53. Murnaghan, F.D. "The compressibility of media under extreme pressures", *Proc. Natl. Acad. Sci.*, **30**(9), pp. 244-247 (1944).
54. Gai, L., Mei, Q., Qin, X., Li, W., Jiang, H., and Duan, X. "Controlled synthesis of anatase TiO_2 octahedra with enhanced photocatalytic activity", *Mater. Res. Bull.*, **48**(11), pp. 4469-4475 (2013).

Biographies

Debashish Dash received the BTech degree in Electronics and Communication Engineering from Silicon Institute of Technology, Bhubaneswar, India, in 2007 and MTech degree in Control and Industrial Automation from NIT, Silchar, in 2013. Also, he completed the PhD degree in Electrical Engineering in 2018 at the National Institute of Technology Silchar, Assam, India. His current research interests include computational physics and modelling and simulation of semiconductor

devices. Currently, he is working as Assistant Professor at Madanapalle Institute of Technology and Science (MITS), Andhra Pradesh, India.

Chandan Kumar Pandey received the BTech degree in Instrumentation and Electronics Engineering from National Institute of Science and Technology, Berhampur, India, in 2008 and MTech degree in Electronics and Communication Engineering from IIT Kharagpur, Kharagpur, in 2014. He is currently working towards the PhD degree in Electrical Engineering at the National Institute of Technology Silchar, Assam, India. His current research interests include modelling and simulation of semiconductor devices and computational physics.

Saurabh Chaudhury received the BTech degree in Electrical Engineering from Regional Engineering College (now NIT) Silchar, India, in 1994, and the MTech and PhD degrees in Microelectronics and VLSI Design from IIT Kharagpur, Kharagpur, India, in 2001 and 2009, respectively. He joined NIT Silchar in 1997 as a lecturer and currently, he is an Associate Professor. He is a reviewer of many international journals including IEEE TNANO, IET, and Elsevier as well as conference journals. His research interests include modelling and simulation of semiconductor devices, low-power VLSI design, carbon nanotube-based FET devices and circuits, digital signal, and image processing.

Susanta Kumar Tripathy received the BTech degree in Electronics and Communication Engineering from Biju Patnaik University of Technology, Odisha, India, in 2003; the MTech in Digital Systems from MNNIT, Allahabad, in 2009; and PhD in Electronics Engineering from IIT (ISM) Dhanbad, India, in 2014. He joined NIT Silchar in 2015 and is now an Assistant Professor. Prior to joining NIT Silchar, he was serving the Sant Longowal Institute of Technology (SLIET), Punjab. He is a reviewer of many international journals including IEEE TNANO, IET, and Elsevier as well as conference journals. His research interests include computational physics of transition materials, chalcopyrite, modelling and simulation of semiconductor devices, carbon nanotube-based FET devices, and circuits.